Supporting Information

Magnetic Behaviour of a Spin-Canted Asymmetric Lanthanide Quinolate Trimer

Lester Batista[a], Sagar Paul[b], Concepcion Molina-Jirón[c,d]*, Juan A. Jaén[e,f], Dieter Fensker[g], Olaf Fuhr[g,h], Mario Ruben[d,g,i]*, Wolfgang Wernsdorfer[b,d]* and Eufemio Moreno-Pineda[b,e,f]*

[a] Universidad de Panamá, Facultad de Ciencias Naturales, Exactas y Tecnología, Depto. Física, 0824, Panamá.

[b] Physikalisches Institut, Karlsruhe Institute of Technology, D-76131, Karlsruhe, Germany.

[c] Universidad de Panamá, Facultad de Ciencias Naturales, Exactas y Tecnología, Depto. de Bioquímica, 0824, Panamá.

[d] Institute of Quantum Materials and Technologies (IQMT), Karlsruhe Institute of Technology (KIT), Hermann-von-Helmholtz-Platz 1, 76344, Eggenstein-Leopoldshafen, Germany.

[e] Universidad de Panamá, Facultad de Ciencias Naturales, Exactas y Tecnología, Depto. de Química-Física, 0824, Panamá.

[f] Universidad de Panamá, Facultad de Ciencias Naturales, Exactas y Tecnología, Grupo de Investigación de Materiales, Panamá, 0824, Panamá.

[g] Institute of Nanotechnology (INT), Karlsruhe Institute of Technology (KIT), Kaiserstraße 12, D-76131 Karlsruhe, Germany.

[h] Karlsruhe Nano Micro Facility (KNMFi), Karlsruhe Institute of Technology (KIT), Kaiserstraße 12, D-76131 Karlsruhe, Germany.

[i] Centre Européen de Sciences Quantiques (CESQ), Institut de Science et d'Ingénierie Supramoléculaires (ISIS), 8 allée Gaspard Monge, BP 70028, 67083, Strasbourg Cedex, France.

*Correspondence to: eufemio.moreno@up.ac.pa; concepcion.molina@up.ac.pa; mario.rube@kit.edu; wolfgang.wernsdorfer@kit.edu

1. EXPERIMENTAL SECTION

1.1. *Synthetic method*

All reactions were carried out under aerobic conditions. Solvents and reagents were used as purchased without additional purification.

Synthesis of [Dy₃(hq)₇(NO₃)₂(H₂O)]: the reaction of $Dy(NO_3)_3 \cdot nH_2O$ (0.548 g, 1.2 mmol)*, 8-hydroxiquinoline (0.464 g, 3.2 mmol) and Et_3N (0.14 mL, 1 mmol) in refluxing acetonitrile (20 mL) for two hours lead to a deep orange solution. The solution was then allowed to cool down to room temperature and filtered. Orange crystals (of X-ray diffraction quality) of **[Dy₃(hq)₇(NO₃)₂(H₂O)]** were obtained after two days of slow evaporation of the solvent in 45% yield (based on the metal content). Elemental analysis Calcd. for ($C_{65}H_{47}Dy_3O_{14}N_{10}$): C, 46.77; H, 2.93; N, 8.95. Found: C = 46.89, H, 2.89, N = 8.83.

*the molar quantity of the Dy(III) salt was calculated based on the hexahydrate Dy(III) salt $(Dy(NO_3)_3 \cdot 6H_2O)$

1.2. *X-ray data collection and structure solution*

Single crystal X-ray diffraction measurements for **[Dy₃(hq)₇(NO₃)₂(H₂O)]** were carried out on a Stoe StadiVari diffractometer with MoK_α radiation (λ = 0.71073 Å). The crystals were mounted on a MiTeGen Microloop using crystallographic perflourether oil and placed in a cryostream. Data were collected using ω scans to give a complete asymmetric unit. The structures were solved and

refined by full-matrix least-squares methods on all F^2 using SHELX-2018 implemented in Olex2. All non-hydrogen atoms were refined anisotropically. Hydrogen atoms were calculated geometrically and were riding on their parent atoms. Full crystallographic details can be found in CIF format: in the Cambridge Crystallographic Data Centre database (CCDC-2354974). These data can be obtained free of charge via www.ccdc.cam.ac.uk/conts/retrieving.html (or from Cambridge Crystallographic Data Centre, 12 Union Road, Cambridge CB21EZ, UK; fax: (+44)1223-336-033; or deposit@ccdc.cam.ac.uk).

1.3. *Magnetic measurements*

Magnetic susceptibility measurements were conducted in a Quantum Design MPMS-XL SQUID magnetometer on polycrystalline materials in the temperature range of 2 - 300 K with an applied DC magnetic field (H_{DC}) of 1 kOe. The DC data were corrected for diamagnetic contributions from the sample holder and eicosane. Core diamagnetic corrections were performed employing Pascal's constants. The AC data was collected in an oscillating magnetic field of 3.5 Oe and frequencies between 1 and 1.5 kHz. Low temperature (0.03 - 5 K) magnetization studies were performed on single crystals employing a µSQUID array at sweep rates between 0.128 and 0.001 T s^{-1}. The time resolution was approximately 1 ms. The magnetic field was applied in different directions of the µSQUID plane with a precision better than 0.1° by driving three orthogonal coils separately. To ensure good thermalisation, each sample was fixed with apiezon grease.

1.4. *Theoretical Calculations*

For the Complete-active-space self-consistent field (CASSCF) calculations for **[Dy$_3$(hq)$_7$(NO$_3$)$_2$(H$_2$O)]**, we employed OpenMolcas[1,2]. CASSCF-SO calculations were performed on the trinuclear Dy(III) system, using the crystallographic coordinates obtained from the SCXRD structures with no further optimisations. For the calculations two Dy(III) ions were substituted by Y(III) at the time. Basis sets from the ANO-RCC library[3–5] were employed with VTZP quality for Dy, VDZP quality for the coordinated N and O atoms, and VDZ quality for all distant atoms, using the second-order DKH transformation[6]. The molecular orbitals (MOs) were optimised in state-averaged CASSCF calculations. For this, the active space was defined by the nine 4f electrons in the seven 4f orbitals of Dy(III). Three calculations were performed independently for each possible spin state, where 21 roots were included for S = 5/2, 224 roots for S = 3/2, and 490 roots for S = 1/2 (RASSCF routine). The wavefunctions obtained from these CASSCF calculations were posteriorly mixed by spin-orbit coupling, where all 21 of the S = 5/2 states, 128 of the S = 3/2 states, and 130 of the S = 1/2 states were included (RASSI routine[7]). The resulting spin-orbit wavefunctions were decomposed into their CF wavefunctions in the $^6H_{15/2}$ basis, employing the SINGLE_ANISO routine[8,9], and the magnetic susceptibility was calculated.

1.5. *Dipolar Matrix*

Dipolar interactions between two S_{eff} = ½ states can be calculated employing the following equation:

$$H_{dip} = \frac{\mu_0 \mu_B^2}{4\pi r^3} - \left[\bar{\bar{g}}_{A(\alpha,\beta,\gamma)} \cdot \bar{\bar{g}}_{B((\alpha,\beta,\gamma))} - 3\left(\bar{\bar{g}}_{A(\alpha,\beta,\gamma)} \cdot \vec{R}\right) \cdot \left(\vec{R}^T \cdot \bar{\bar{g}}_{B(\alpha,\beta,\gamma)}\right) \right]$$

where µ$_B$ is the Bohr magneton, μ_0 the vacuum permittivity, r is the Ln···Ln distance obtained from crystal structures. $\bar{\bar{g}}_{A/B}$ is the g-matrix of ion A and B, and $\vec{R}$ is the directional unit vector

between the two ions, based on the CASSCF results. The angles of the rotation matrix are the Euler angles, obtained from the CASSCF results, using the Z-Y'-Z" convention according to the following equations:

$$\bar{\bar{R}}_{Z(\alpha)} = \begin{pmatrix} \cos\alpha & -\sin\alpha & 0 \\ \sin\alpha & \cos\alpha & 0 \\ 0 & 0 & 1 \end{pmatrix}$$

$$\bar{\bar{R}}_{Y(\beta)} = \begin{pmatrix} \cos\beta & 0 & \sin\beta \\ 0 & 1 & 0 \\ -\sin\beta & 0 & \cos\beta \end{pmatrix}$$

$$\bar{\bar{R}}_{Z''(\gamma)} = \begin{pmatrix} \cos\gamma & -\sin\gamma & 0 \\ \sin\gamma & \cos\gamma & 0 \\ 0 & 0 & 1 \end{pmatrix}$$

$$\bar{\bar{R}}_{i(\alpha,\beta,\gamma)} = \bar{\bar{R}}_{Z(\alpha)} \cdot \bar{\bar{R}}_{Y(\beta)} \cdot \bar{\bar{R}}_{Z''(\gamma)}$$

$$\bar{\bar{g}}_{i(\alpha,\beta,\gamma)} = \bar{\bar{R}}_{i(\alpha,\beta,\gamma)} \cdot \bar{\bar{g}}_i \cdot \bar{\bar{R}}_{i(\alpha,\beta,\gamma)}^T$$

For the calculation of the dipolar matrix, the reference frame was chosen as shown in Figure S5.

The g-values were used as obtained from CASSCF-SO calculations, which are based on the $S_{eff} = \dfrac{1}{2}$ formalism:

$$\bar{\bar{g}}_{Dy(1)} = \begin{pmatrix} 0 & 0 & 0 \\ 0 & 0 & 0 \\ 0 & 0 & 19.7 \end{pmatrix}; \quad \bar{\bar{g}}_{Dy(2)} = \begin{pmatrix} 1.2 & 0 & 0 \\ 0 & 2.5 & 0 \\ 0 & 0 & 15.9 \end{pmatrix}; \quad \bar{\bar{g}}_{Dy(3)} = \begin{pmatrix} 1.3 & 0 & 0 \\ 0 & 2.4 & 0 \\ 0 & 0 & 16.1 \end{pmatrix}$$

These three ions are connected by a unit vector of the form:

$$\vec{R}_{1-2} = \begin{pmatrix} 0.23 \\ 0.53 \\ 0.82 \end{pmatrix} \text{ and } \vec{R}_{2-3} = \begin{pmatrix} 0.58 \\ 0.67 \\ 0.46 \end{pmatrix}$$

Thus, this leads to a dipolar matrix for Dy(1) and Dy(2) Dy(III) ions separated by a distance of 3.5592(6) Å and with $\alpha_{Dy(1)} = 21°$, $\beta_{Dy(1)} = 37°$ and $\gamma_{Dy(1)} = 164°$ and $\alpha_{Dy(2)} = -78°$, $\beta_{Dy(2)} = 87°$ and $\gamma_{Dy(2)} = -53°$, while for Dy(3) and Dy(2) Dy(III) the distance is 3.5120(6) Å and with $\alpha_{Dy(3)} = 121°$, $\beta_{Dy(3)} = 55°$ and $\gamma_{Dy(3)} = 161°$. The obtained dipolar matrix for Dy$_{1-2}$ has the form (for an +J Hamiltonian):

$$J_{Dy1-2}^{dip} = \begin{pmatrix} 0.430 & -1.818 & -0.199 \\ 0.165 & -0.698 & -0.076 \\ 0.612 & -2.585 & -0.283 \end{pmatrix} \text{ cm}^{-1}$$

while for Dy$_{2-3}$ has the form (for an +J Hamiltonian)

$$J_{Dy2-3}^{dip} = \begin{pmatrix} 0.208 & -0.218 & -0.156 \\ -0.380 & -0.134 & -0.254 \\ -0.051 & -0.048 & -0.075 \end{pmatrix} \text{ cm}^{-1}$$

Which for a $J = 15/2$ are:

$$J_{Dy1-2}^{dip} = \begin{pmatrix} 1.91 \times 10^{-2} & -8.08 \times 10^{-2} & -8.84 \times 10^{-3} \\ 7.34 \times 10^{-3} & -3.10 \times 10^{-2} & -3.39 \times 10^{-3} \\ 2.72 \times 10^{-2} & -1.15 \times 10^{-1} & -1.26 \times 10^{-2} \end{pmatrix} cm^{-1}$$

$$J_{Dy2-3}^{dip} = \begin{pmatrix} 9.27 \times 10^{-3} & -9.70 \times 10^{-3} & -6.94 \times 10^{-3} \\ -1.69 \times 10^{-2} & -5.96 \times 10^{-3} & -1.13 \times 10^{-2} \\ -2.28 \times 10^{-3} & 2.12 \times 10^{-3} & -3.34 \times 10^{-3} \end{pmatrix} cm^{-1}$$

Projecting the strongest component of the dipolar matrices (i.e., -8.08 $\times$ 10^{-2}) onto a S = 5/2 state is ~0.73 cm^{-1}.

Table S1. Crystal Data and Structure Refinements for **[Dy$_3$(hq)$_7$(NO$_3$)$_2$(H$_2$O)·2.5(CH$_3$CN)]**

Formula	C$_{68}$H$_{51.5}$Dy$_3$N$_{11.5}$O$_{14}$
Fw	1741.20
T(K)	180
crystal system	triclinic
space group	$P\bar{1}$
a，Å	11.6383(4)
b，Å	16.6621(6)
c，Å	18.2109(6)
α，deg	76.207(3)
β，deg	72.362(3)
γ，deg	88.591(3)
V (Å^3)	3264.0(2)
Z	2
$\rho_{Calcd.}$ (mg·m^{-3})	1.772
μ (mm^{-1})	3.474
R_{int}	0.0400
GOF on F^2	0.797
R_1, wR_2 (I > 2σ(I))[a]	R_1 = 0.0318, wR_2 = 0.0502
R_1, wR_2(all data)	R_1 = 0.0575, wR_2 = 0.0523
CCDC number	2354974

Table S2. Continuous shaped measures (CShM) for {Ln$_3$} obtained using SHAPE.

CShM	Dy(1)	CShM	Dy(2)	CShM	Dy(3)
OP-8	30.513	OP-8	27.576	EP-9	35.964
HPY-8	21.381	HPY-8	21.471	OPY-9	21.923
HBPY-8	16.624	HBPY-8	17.110	HBPY-9	16.336
CU-8	10.533	CU-8	11.711	JTC-9	15.492
SAPR-8	1.364	SAPR-8	1.129	JCCU-9	9.496
TDD-8	1.676	TDD-8	2.751	CCU-9	7.957
JGBF-8	14.953	JGBF-8	15.727	JCSAPR-9	3.954
JETBPY-8	27.545	JETBPY-	25.536	CSAPR-9	2.808
JBTPR-8	2.765	JBTPR-8	2.931	JTCTPR-9	4.105
BTPR-8	2.287	BTPR-8	2.136	TCTPR-9	2.232
JSD-8	4.349	JSD-8	5.173	JTDIC-9	12.036
TT-8	11.291	TT-8	12.073	HH-9	8.826
ETBPY-8	21.839	ETBPY-8	21.393	MFF-9	3.254

OP-8 = (D_{8h}) Octagon
HPY-8 = (C_{7v}) Heptagonal pyramid
HBPY-8 = (D_{6h}) Hexagonal bipyramid
CU-8 = (O_h) Cube
SAPR-8 = (D_{4d}) Square antiprism
TDD-8 = (D_{2d}) Triangular dodecahedron
JGBF-8 = (D_{2d}) Johnson gyrobifastigium J26
JETBPY-8 = (D_{3h}) Johnson elongated triangular bipyramid J14
JBTPR-8 = (C_{2v}) Biaugmented trigonal prism J50
BTPR-8 = (C_{2v}) Biaugmented trigonal pris
JSD-8 = (D_{2d}) Snub diphenoid J84
TT-8 = (T_d) Triakis tetrahedron
ETBPY-8 = (D_{3h}) Elongated trigonal bipyramid
EP-9 = (D_{9h}) Enneagon
OPY-9 = (C_{8v}) Octagonal pyramid
HBPY-9 = (D_{7h}) Heptagonal bipyramid
JTC-9 =4 (C_{3v}) Johnson triangular cupola J3
JCCU-9 = (C_{4v}) Capped cube J8
CCU-9 = (C_{4v}) Spherical-relaxed capped cube
JCSAPR-9 = (C_{4v}) Capped square antiprism J10
CSAPR-9 = (C_{4v}) Spherical capped square antiprism
JTCTPR-9 = (D_{3h}) Tricapped trigonal prism J51
TCTPR-9 = (D_{3h}) Spherical tricapped trigonal prism
JTDIC-9 = (C_{3v}) Tridiminished icosahedron J63
HH-9 = (C_{2v}) Hula-hoop
MFF-9 = (Cs) Muffin

Table S3. Electronic structure of individual Dy(1) fragment calculated with CASSCF-SO using solid-state geometry for $[Dy_3(hq)_7(NO_3)_2(H_2O)]$.

Energy (cm^{-1})	g_x	g_y	g_z
0.0	0.0031	0.0031	19.7313
146.675	0.02577	0.0283	16.8559
273.297	0.25712	0.2877	13.8209
356.719	2.2044	2.7268	10.3390
397.772	3.8330	5.7488	10.4314
441.506	0.5183	1.4976	15.5795
462.338	0.6618	1.9093	18.1526
625.039	0.0031	0.0082	19.7588

Table S4. Electronic structure of individual Dy(2) fragment calculated with CASSCF-SO using solid-state geometry for $[Dy_3(hq)_7(NO_3)_2(H_2O)]$.

Energy (cm^{-1})	g_x	g_y	g_z
0.0	1.17528	2.5234	15.8724
14.523	3.1106	6.6821	9.2494
39.999	1.0721	4.4142	12.6510
58.65	0.1835	2.2840	10.7784
99.578	2.0358	2.5718	15.5003
142.308	1.03259	5.1647	10.8812
198.017	1.4253	3.3889	16.5116
416.435	0.0230	0.0539	19.6368

Table S5. Electronic structure of individual Dy(3) fragment calculated with CASSCF-SO using solid-state geometry for $[Dy_3(hq)_7(NO_3)_2(H_2O)]$.

Energy (cm^{-1})	g_x	g_y	g_z
0.0	1.3454	2.3672	16.1306
34.729	1.5948	4.4755	10.5981
75.518	0.9328	4.5785	12.3275
102.514	2.6088	5.1682	8.9580
169.739	0.5605	2.9019	12.8775
188.479	1.5394	4.7664	11.7529
245.130	2.4503	3.6999	10.2534
288.837	0.97036	3.8682	16.1998

Table S6. Crystal field Hamiltonian is given as $\hat{H}_{CF} = \sum_{k,q} B_k^q O_k^q$ and the extended Stevens operator coefficients B_k^q are extracted from CASSCF calculations for **[Dy₃(hq)₇(NO₃)₂(H₂O)]**. (the calculation was performed for the individual centers).

| | | B_k^q | | |
k	q	Dy(1)	Dy(2)	Dy(3)
2	-2	0.0775	-0.49161	-0.18992
2	-1	0.90003	-0.29656	-0.8264
2	0	-2.659	0.06266	-0.25298
2	1	-2.57459	-4.57497	0.7291
2	2	0.97996	0.21695	1.05765
4	-4	-0.00261	0.01533	0.00823
4	-3	0.01068	0.01453	-0.02872
4	-2	0.00569	-0.00654	-0.00438
4	-1	-0.00563	-0.00567	-0.01251
4	0	-0.00387	-0.00496	-0.00322
4	1	0.00856	-0.01881	-0.0079
4	2	0.01379	0.01918	0.00897
4	3	-0.08847	-0.04075	-0.00976
4	4	0.01157	0.01631	0.0205
6	-6	-2.87047E-6	-1.68086E-4	-9.5566E-5
6	-5	-2.15146E-4	-3.26232E-4	-2.37239E-4
6	-4	-6.83192E-5	-4.76288E-6	2.82357E-4
6	-3	-1.02898E-4	1.34513E-4	1.81636E-4
6	-2	1.41136E-5	9.95391E-5	1.88887E-4
6	-1	-2.30195E-6	1.0654E-4	9.33672E-5
6	0	1.43456E-5	-8.66577E-6	-1.74113E-5
6	1	5.45324E-5	2.74291E-4	-2.36552E-4
6	2	-6.07279E-5	2.15707E-5	-1.1768E-5
6	3	-4.81681E-5	-2.29162E-4	-1.02529E-4
6	4	1.82462E-4	1.41755E-4	6.33668E-5
6	5	-6.3016E-4	-5.58246E-4	-1.22168E-5
6	6	4.19208E-5	2.04249E-5	1.14044E-4

Table S7. Relaxation fitting parameters from the least-square fitting of the Cole-Cole plots **for [Dy₃(hq)₇(NO₃)₂(H₂O)]** under a zero-dc field at 2.0-6.8 K according to the generalized Debye model.

| T / K	τ / s	χ_S / cm^{3}mol^{-1}	χ_T / cm^{3}mol^{-1}	α
1.9998	0.00120(2)	6.37(3)	10.55(1)	0.176(8)
2.1878	0.00120(2)	6.09(2)	9.94(1)	0.173(8)
2.3999	0.00119(2)	5.75(2)	9.24(1)	0.171(7)
2.5997	0.00118(2)	5.47(2)	8.68(1)	0.169(7)
2.7996	0.00117(2)	5.21(2)	8.18(1)	0.168(7)
2.9994	0.00117(2)	4.98(2)	7.74(1)	0.167(7)
3.1989	0.00116(2)	4.76(2)	7.34(1)	0.166(7)
3.3997	0.00115(2)	4.56(2)	6.99(1)	0.166(7)
3.5993	0.00115(2)	4.38(1)	6.66(1)	0.163(7)
3.7994	0.00114(2)	4.22(1)	6.37(1)	0.163(6)
3.9969	0.00113(2)	4.06(1)	6.10(1)	0.163(7)
4.0269	0.00112(1)	3.92(1)	5.86(1)	0.161(7)
4.1999	0.00108(1)	3.77(1)	5.63(1)	0.163(7)
4.5981	0.00106(1)	3.63(1)	5.421(4)	0.166(5)
4.7993	0.00102(1)	3.51(1)	5.243(4)	0.167(5)
4.9992	0.00100(1)	3.41(1)	5.062(4)	0.164(5)
5.3989	9.47(1)E-4	3.21(1)	4.737(3)	0.162(5)
5.7992	8.72(9)E-4	3.04(1)	4.454(3)	0.159(5)
6.1987	7.78(3)E-4	2.89(1)	4.204(2)	0.158(4)
6.5983	6.61(6)E-4	2.74(1)	3.981(2)	0.164(5)
6.9984	5.36(6)E-4	2.61(1)	3.782(2)	0.172(5)
7.3902	4.12(6)E-4	2.49(1)	3.604(2)	0.188(6)
7.7985	3.02(6)E-4	2.39(1)	3.444(2)	0.210(7)
8.1988	2.21(7)E-4	2.31(2)	3.298(2)	0.229(9)
8.5984	1.71(8)E-4	2.28(2)	3.162(2)	0.23(1)
8.9981	1.42(7)E-4	2.27(2)	3.037(2)	0.22(1)
9.3978	1.18(6)E-4	2.27(2)	2.922(2)	0.20(1)
9.7985	9.35(5)E-5	2.24(2)	2.816(1)	0.19(1)
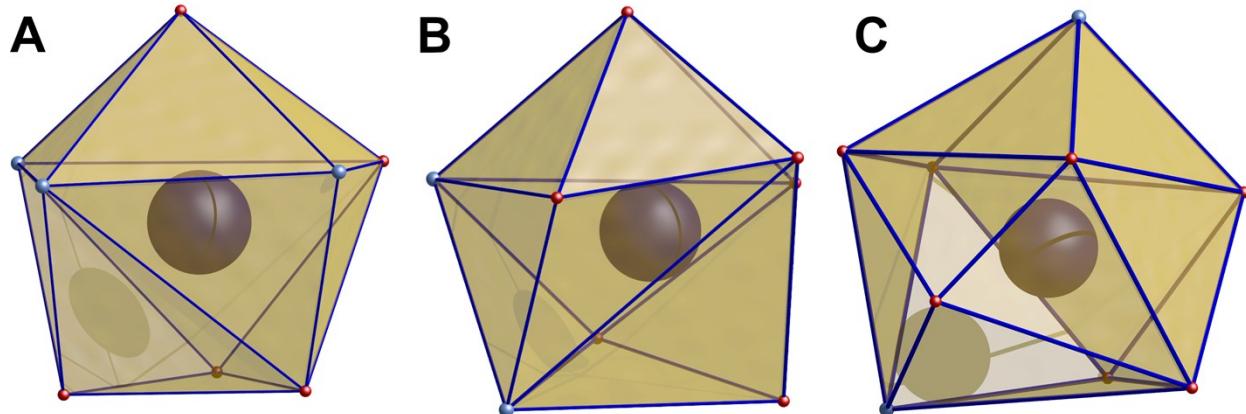
Figure S1. Polyhedral representation of the coordination environment for (**A**) Dy(1); (**B**) Dy(2); and (**C**) Dy(3).
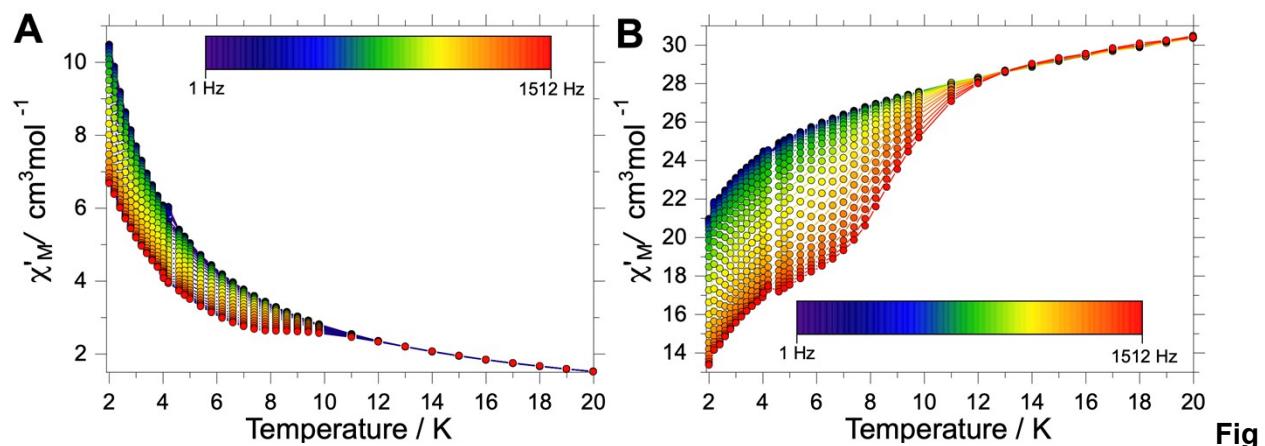

Figure S2. $\chi_M'(T)$ and $\chi_M'T(T)$ data for **[Dy$_3$(hq)$_7$(NO$_3$)$_2$(HO$_2$)]**.
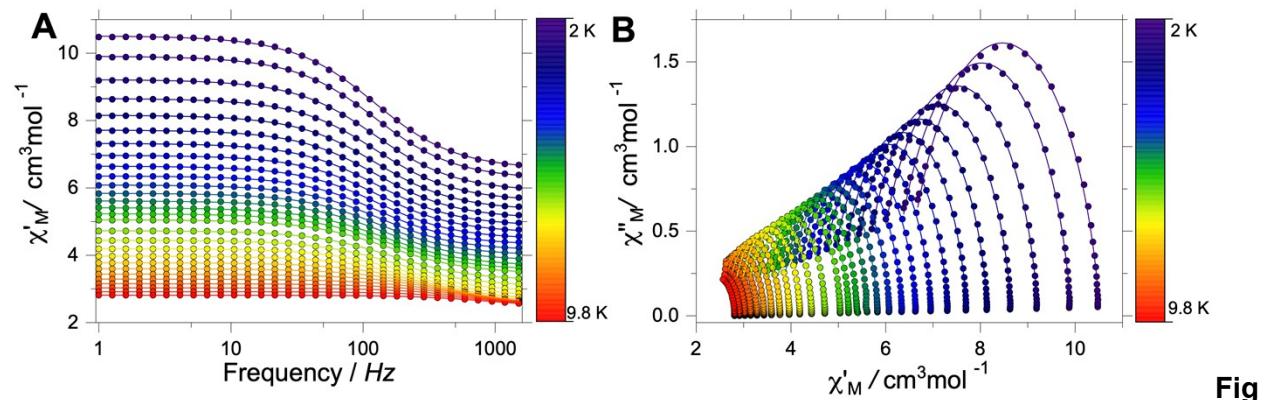
Figure S3. $\chi_M'(\nu)$ and Cole-Cole data for **[Dy$_3$(hq)$_7$(NO$_3$)$_2$(H$_2$O)]**. Solid lines are the fit to a generalised Debye process.
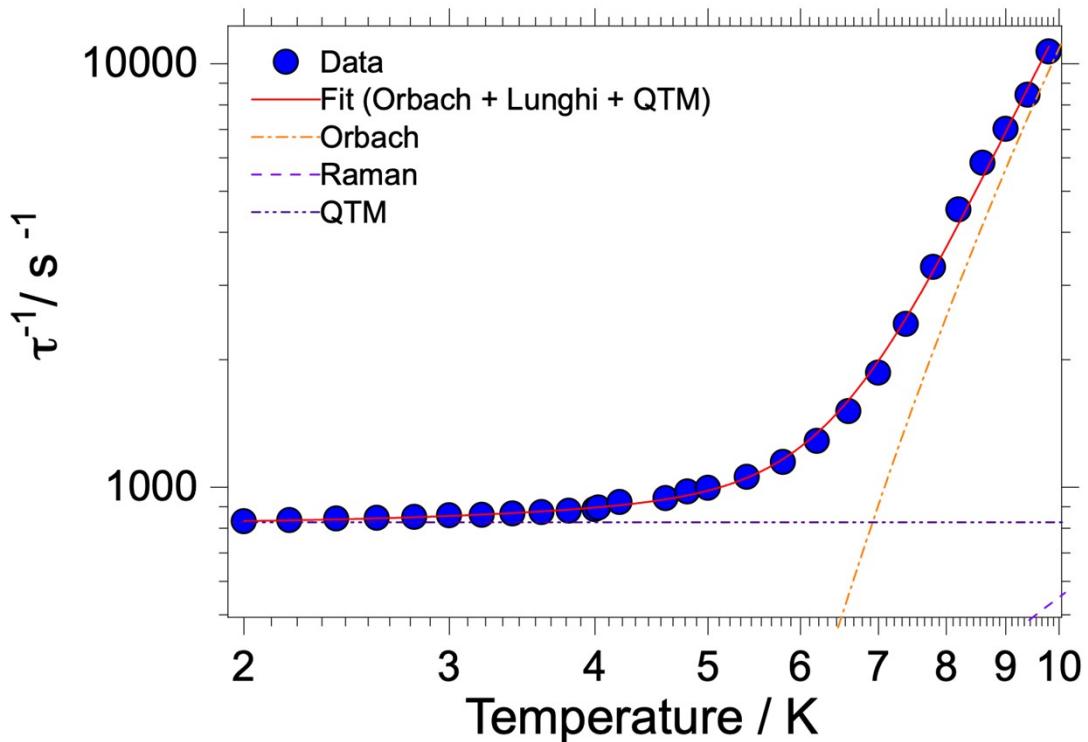
Figure S4. $\tau(T)$ experimental data (blue symbols) for **[Dy$_3$(hq)$_7$(NO$_3$)$_2$(H$_2$O)]** obtained from the generalised Debye model and the fit to a model comprising the Raman process proposed by Lunghi, Orbach and QTM processes (solid line) and their decomposition.
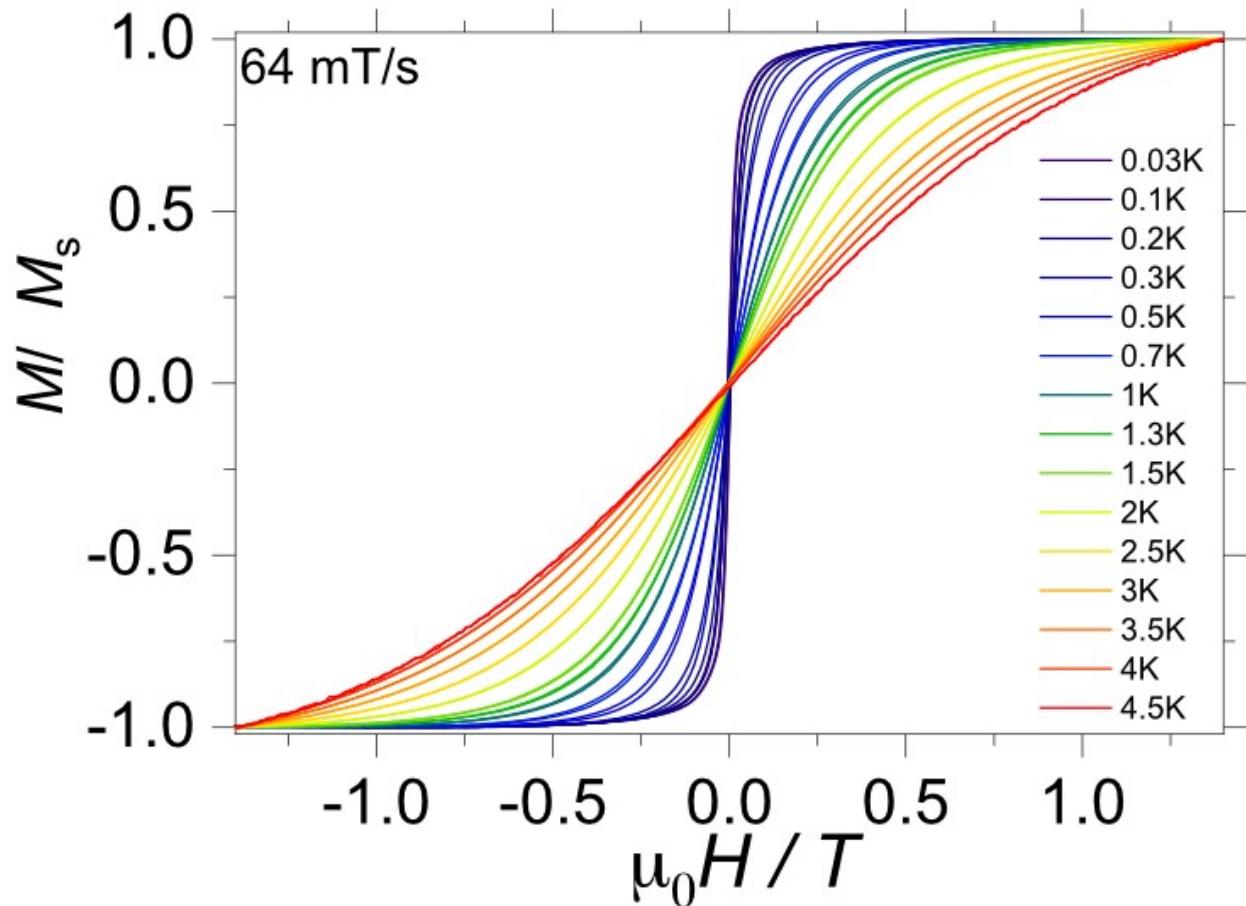
Figure S5. Temperature-dependent studies for sweeping rate of 64 mT/s and temperatures between 30 mK and 4.5 K.
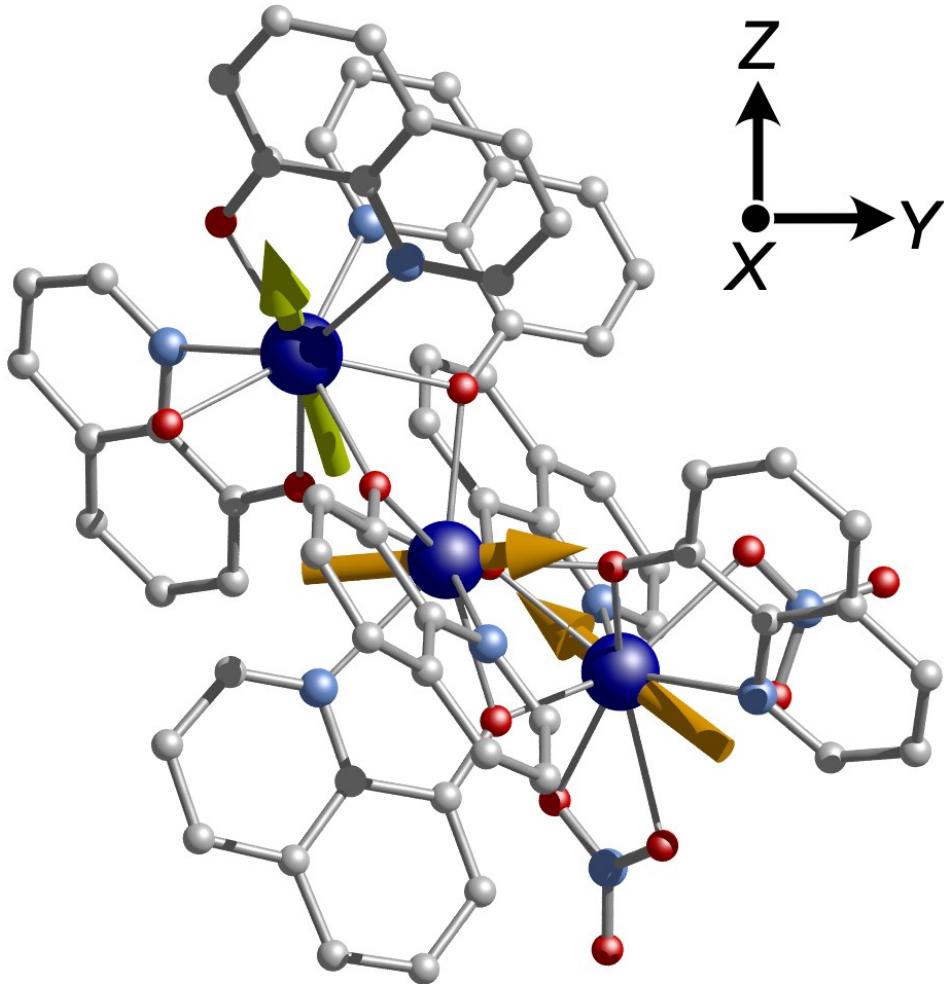
Figure S6. Reference frame of **[Dy₃(hq)₇(NO₃)₂(H₂O)]** employed for the dipolar field calculations.

References

1   I. Fdez. Galván, M. Vacher, A. Alavi, C. Angeli, F. Aquilante, J. Autschbach, J. J. Bao, S. I. Bokarev, N. A. Bogdanov, R. K. Carlson, L. F. Chibotaru, J. Creutzberg, N. Dattani, M. G. Delcey, S. S. Dong, A. Dreuw, L. Freitag, L. M. Frutos, L. Gagliardi, F. Gendron, A. Giussani, L. González, G. Grell, M. Guo, C. E. Hoyer, M. Johansson, S. Keller, S. Knecht, G. Kovačević, E. Källman, G. Li Manni, M. Lundberg, Y. Ma, S. Mai, J. P. Malhado, P. Å. Malmqvist, P. Marquetand, S. A. Mewes, J. Norell, M. Olivucci, M. Oppel, Q. M. Phung, K. Pierloot, F. Plasser, M. Reiher, A. M. Sand, I. Schapiro, P. Sharma, C. J. Stein, L. K. Sørensen, D. G. Truhlar, M. Ugandi, L. Ungur, A. Valentini, S. Vancoillie, V. Veryazov, O. Weser, T. A. Wesołowski, P. O. Widmark, S. Wouters, A. Zech, J. P. Zobel and R. Lindh, *J Chem Theory Comput*, 2019, **15**, 5925–5964.

2   G. Li Manni, I. Fdez. Galván, A. Alavi, F. Aleotti, F. Aquilante, J. Autschbach, D. Avagliano, A. Baiardi, J. J. Bao, S. Battaglia, L. Birnoschi, A. Blanco-González, S. I. Bokarev, R. Broer, R. Cacciari, P. B. Calio, R. K. Carlson, R. Carvalho Couto, L. Cerdán, L. F. Chibotaru, N. F. Chilton, J. R. Church, I. Conti, S. Coriani, J. Cuéllar-Zuquin, R. E.

Daoud, N. Dattani, P. Decleva, C. de Graaf, M. G. Delcey, L. De Vico, W. Dobrautz, S. S. Dong, R. Feng, N. Ferré, M. Filatov, L. Gagliardi, M. Garavelli, L. González, Y. Guan, M. Guo, M. R. Hennefarth, M. R. Hermes, C. E. Hoyer, M. Huix-Rotllant, V. K. Jaiswal, A. Kaiser, D. S. Kaliakin, M. Khamesian, D. S. King, V. Kochetov, M. Krośnicki, A. A. Kumaar, E. D. Larsson, S. Lehtola, M. B. Lepetit, H. Lischka, P. López Ríos, M. Lundberg, D. Ma, S. Mai, P. Marquetand, I. C. D. Merritt, F. Montorsi, M. Mörchen, A. Nenov, V. H. A. Nguyen, Y. Nishimoto, M. S. Oakley, M. Olivucci, M. Oppel, D. Padula, R. Pandharkar, Q. M. Phung, F. Plasser, G. Raggi, E. Rebolini, M. Reiher, I. Rivalta, D. Roca-Sanjuán, T. Romig, A. A. Safari, A. Sánchez-Mansilla, A. M. Sand, I. Schapiro, T. R. Scott, J. Segarra-Martí, F. Segatta, D. C. Sergentu, P. Sharma, R. Shepard, Y. Shu, J. K. Staab, T. P. Straatsma, L. K. Sørensen, B. N. C. Tenorio, D. G. Truhlar, L. Ungur, M. Vacher, V. Veryazov, T. A. Voß, O. Weser, D. Wu, X. Yang, D. Yarkony, C. Zhou, J. P. Zobel and R. Lindh, *J Chem Theory Comput*, 2023, **19**, 6933–6991.

3   B. O. Roos, R. Lindh, P. Å. Malmqvist, V. Veryazov and P. O. Widmark, *Journal of Physical Chemistry A*, 2004, **108**, 2851–2858.

4   B. O. Roos, R. Lindh, P.-Å. Malmqvist, V. Veryazov, P.-O. Widmark and A. C. Borin, *J Phys Chem A*, 2008, **112**, 11431–11435.

5   P.-O. Widmark, P.-□ke Malmqvist and B. O. Roos, *Theor Chim Acta*, 1990, **77**, 291–306.

6   D. Peng and K. Hirao, *J Chem Phys*, 2009, **130**, 044102.

7   P. Å. Malmqvist, B. O. Roos and B. Schimmelpfennig, *Chem Phys Lett*, 2002, **357**, 230–240.

8   L. F. Chibotaru and L. Ungur, *J Chem Phys*, 2012, **137**, 064112.

9   L. Ungur and L. F. Chibotaru, *Chemistry - A European Journal*, 2017, **23**, 3708–3718.